

Extended data

Gate voltage modulation of the superconducting state in a degenerate semiconductor

Bikash C. Barik,¹ Himadri Chakraborti,^{1,2} Buddhadeb Pal,^{1,3} Aditya K. Jain,^{1,4} Swagata Bhunia,¹ Sounak Samanta,¹ Apurba Laha,⁵ Suddhasatta Mahapatra,¹ and K. Das Gupta^{1,*}

¹*Department of Physics, Indian Institute of Technology Bombay, India*

²*SPEC, CEA, CNRS, Universite Paris-Saclay, CEA Saclay, 91191 Gif sur Yvette Cedex France*

³*Indian Association for the Cultivation of Science, Kolkata, 700032, India*

⁴*Department of Physics, Royal Holloway, University of London, Egham, Surrey, TW20 0EX, UK*

⁵*Department of EE, Indian Institute of Technology Bombay, India, India*

I. INDIUM NITRIDE SAMPLES FABRICATION PROCESS

Here we give a detailed idea about the growth technique, fabrication processes and different characterization techniques of InN samples that we have used in our experiment. InN samples were grown in plasma-assisted molecular beam epitaxy (PA-MBE) system (RIBER compact 21) with RIBER Addon radio frequency plasma source for the active N species on sapphire substrates and this growth was done by Kankat Ghosh/Swagata Bhunia [1]. First GaN layer of ~ 300 nm is grown on the sapphire substrate and then ~ 300 nm InN is grown on the top of that. To make the channel of InN, etching needs to be done. The sample goes through different stages during fabrication which are mentioned below.

Fabrication steps

All the fabrication steps are described below.

- Substrate preparation: Cleaning of the sample with acetone and isopropyl alcohol.
- Deposition of 100nm Al_2O_3 as a hard mask using atomic layer deposition (ALD).
- Hall bar pattern by photolithography. It includes:
 - Spin coating on photoresist using S1813 positive photoresist.
 - Exposing to UV light through a mask using mask aligner (MA400).
 - Development in the MF319 developer solution.
- Etching Al_2O_3 in HF solution.
- Dry etch of InN in reactive etching system (RIE).
- Removal of photoresist and Al_2O_3 .
- Patterning contact by photolithography.
- Metals (Ti/Au) deposition by thermal evaporation process of thickness 20nm and 100nm.
- Liftoff in acetone.
- Mounting in a Leadless chip carrier (LCC) and bonding is done by a wire bonder.
- Deposition of ionic liquid on the hall bar and curing for 48 hours at high vacuum (Pressure $< 1 \times 10^{-5}$ mbar) and at temperature 110°C .

* kdasgupta@phy.iitb.ac.in

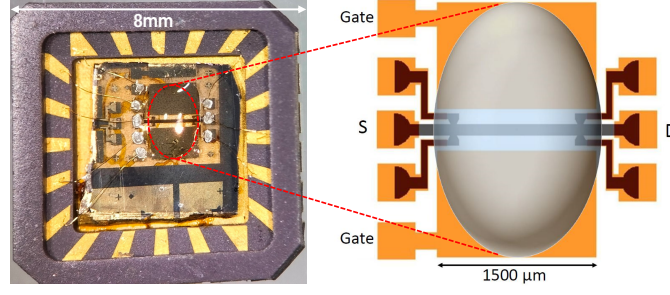


FIG. 1. Actual InN device, ionic liquid deposited portion is shown in the red-dashed line (left). Schematic diagram of the device is shown. (right)

II. TRANSISTOR CHARACTERISTICS

Fig. 2 shows the transfer characteristics of the IL-gated InN at room temperature. To maintain a constant source-drain voltage of 100 mV (V_{SD}), a DC voltage source is used. The gate voltage (V_G) is swept in 0.1 V steps using another voltage Source. Notably, different settling times—ranging from 30 s to 240 s—are set during the gate voltage sweep. These settling times allow for the system to stabilize after voltage changes. The measurement of gate leakage current is crucially smaller by approximately three orders of magnitude than the source-drain current. This substantial difference ensures that gate leakage doesn't impact on the device's performance. The observed trend in the data indicates n -type characteristics, as I_{SD} increases with the application of increasingly positive V_G .

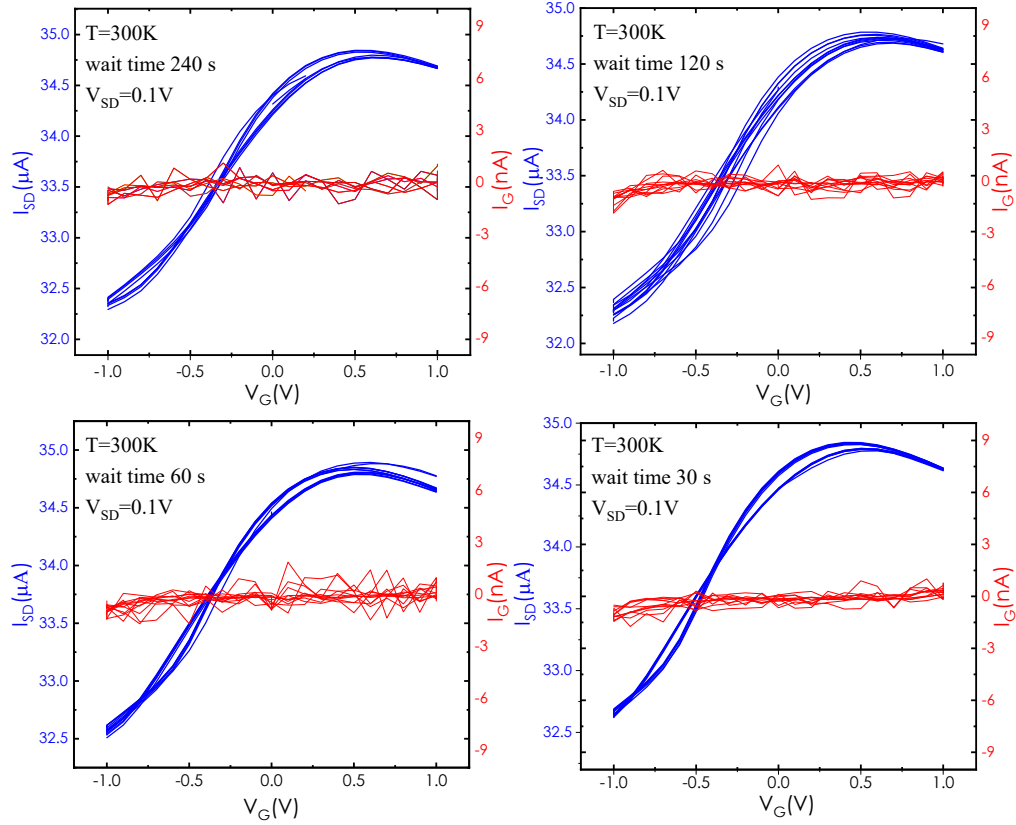


FIG. 2. At $T=300$ K, the transfer characteristics exhibit a nearly hysteresis-free nature across various settling times (InNB3601 sample).

III. BEHAVIOUR OF AN IONIC LIQUID GATE

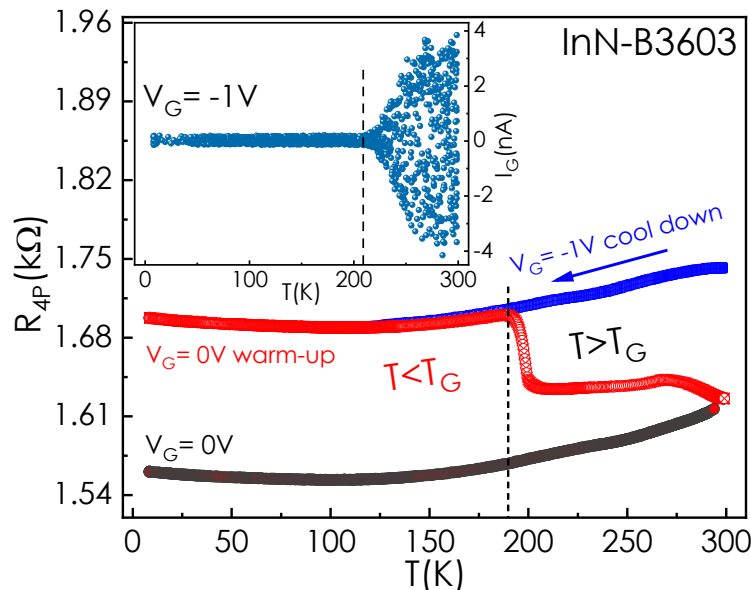


FIG. 3. The glass transition temperature phenomenon is investigated by applying a gate voltage of $V_G = -1$ V and subsequently removing the gate voltage at a low temperature of 10 K. The resulting observation of a significant jump in resistance serves as a clear indicator of the glass transition temperature associated with the ionic liquid. The inset depicts the recorded gate leakage current at a gate voltage, $V_G = -1$ V, providing a compelling illustration of the phenomenon associated with the freezing of ions.

Fig 3 shows the striking difference between the behaviour of an ionic liquid gate and a conventional dielectric gate. The ionic motion within the liquid starts to undergo a slowdown below approximately ~ 230 K. Furthermore, below a specific temperature marked as the glass transition temperature (T_G), the ions associated with the ionic liquid experience complete immobilization. [2][3]. A gate voltage $V_G = -1$ V was applied and the sample was cooled down to 10 K. The resistance follows the blue curve. The corresponding gate leakage current is illustrated in the inset. At 10 K the voltage source is set to zero and disconnected. The sample is then allowed to warm up but continues to behave as if the gate voltage is still present. When the glass transition temperature (T_G) is reached, the ions in the ionic liquid regain their motion and adjust to the absence of the external field, at this point one begins to see considerable fluctuations in the gate leakage current. This happens over a range of $T \approx 180 - 200$ K which corresponds well to the known value of T_G of DEME-TFSI. Changing the gate voltage will have the desired effect only if done at $T \gg T_G$. In our experiments we always allowed the sample to warm up to room temperature for setting V_G .

IV. CAPACITANCE MEASUREMENTS

A. From gate response

The time response of the electrical double layer (EDL) gate in the InN film to a step change in gate bias voltage (V_G) has been investigated. The results are illustrated in Fig. 4 depicting the growth and decay curves for various gate voltages.

The figures showcase the InN film resistance's time response to negative gate voltages, revealing distinct growth and decay curves. The time scale for capacitor charging and discharging is extracted from these curves. Notably, for $V_G = -0.5$ V, the fast time scale (τ) is found to be consistent for both growth (6.9 s) and decay (9.5 s) processes, indicating the charging and discharging of the EDL. The gate leakage current suggests that gate charging occurs through an equivalent resistance (R_G) of approximately $\simeq 700$ M Ω .

The time constant of the charging and discharging curves ($\tau = RC$) is utilized to determine the gate capacitance (C_G). For $V_G = -0.5$ V, the calculated gate capacitance is approximately ~ 8.52 $\mu\text{F}/\text{cm}^2$. A similar analysis for $V_G = -1$ V yields a gate capacitance of around ~ 10.4 $\mu\text{F}/\text{cm}^2$, with gate charging occurring through an equivalent

resistance of $R_G \simeq 400 \text{ M}\Omega$, as depicted in figure 4. The gate capacitance values measured by this technique match well with the capacitance derived from Hall measurements i.e $8.8 \text{ }\mu\text{F}/\text{cm}^2$ (see text).

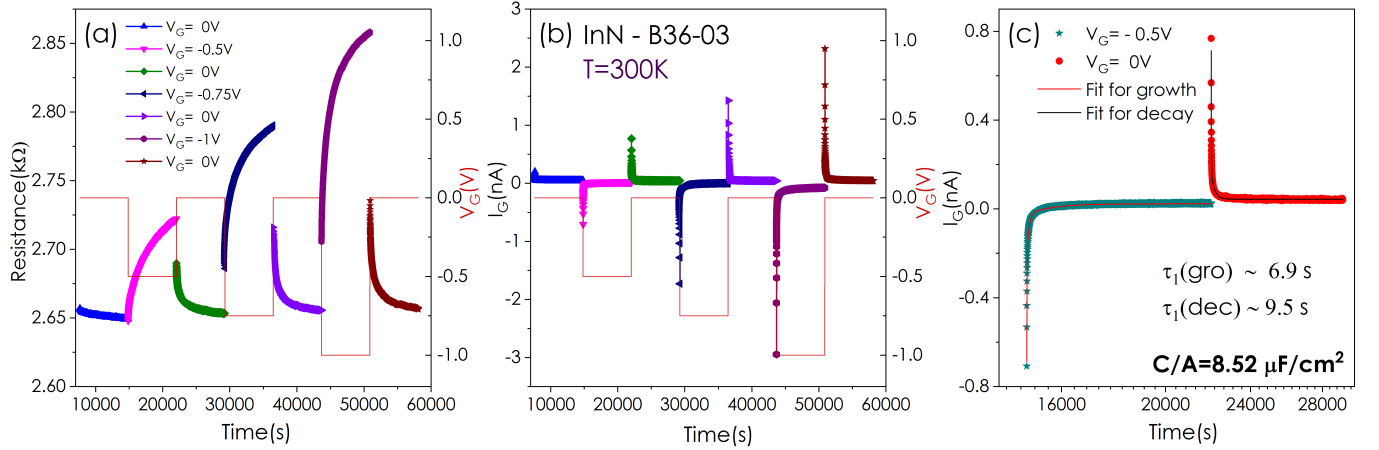


FIG. 4. (a) Transient response of InN film resistance to the negative gate voltages. (b) The gate leakage current of corresponding gate voltages are shown. (c) Transient response of the gate leakage current for $V_G = -0.5 \text{ V}$. The calculated value of the capacitance from the fitting is shown.

B. From electrochemical impedance analysis

We used electrochemical impedance spectroscopy to study the frequency dependence impedance as well as to measure the EDL capacitance [4][5]. We measured the impedance of gated InN thin film as a function of frequency for different applied gate voltages from 37 mHz to 2 kHz. Impedance measurements are performed using two lock-in amplifiers. The low-frequency measurement is done by configuring a high time constant of 30 s and a corresponding settling time of 300 s. The gate voltage is applied using a voltage source. Lock-in amplifiers do not give the value of impedance directly but it can be calculated using the following relations.

$$Z = \frac{V_S}{I_S} = \frac{V_S}{V_R} \times R = R \times \left(\frac{V'_S + jV''_S}{|V_R|} \right) \quad (1)$$

$$Z = R \times \left(\frac{V'_S + jV''_S}{\sqrt{(V'_R)^2 + (V''_R)^2}} \right) \quad (2)$$

$$Z' = R \times \frac{V'_S}{\sqrt{(V'_R)^2 + (V''_R)^2}} \quad (3)$$

$$Z'' = R \times \left(\frac{V''_S}{\sqrt{(V'_R)^2 + (V''_R)^2}} \right) \quad (4)$$

Where V_S and V_R are the voltage across the InN sample and standard $1\text{ k}\Omega$ resistor respectively. $1 \text{ k}\Omega$ is used to measure the current through the sample. Z' and Z'' are real and imaginary parts of the impedance and Z is the total impedance of the system. The model shown in the inset of Fig. 5 is the capacitive coupling between InN film with resistance R and the ionic liquid with resistance R_{IL} . A constant current $10 \text{ }\mu\text{A}$ is applied by applying 2.5 V from the lock-in's internal oscillator through a $250 \text{ k}\Omega$ resistor in series. The magnitude of the impedance between the source and drain can be calculated. Fig. 5 show the impedance of the InN sample for different applied gate voltages.

In the model shown in the inset of Fig. 5, the capacitance near the gate-liquid interface is taken to be approximately 13 times greater than the channel-liquid capacitance. This ratio is justified by the substantial difference in the areas

of the gate electrode and the channel, indicating that the majority of the potential will be distributed across the working electrode, i.e. the source and drain regions. Consequently, the need for a reference electrode is eliminated. The circuit model, as illustrated in the inset of Fig. 5, is fitted for impedance analysis. Notably, a satisfactory fit is achieved using this model up to 1 kHz, and the resulting values for capacitance per unit area and R_{IL} are detailed in Table I.

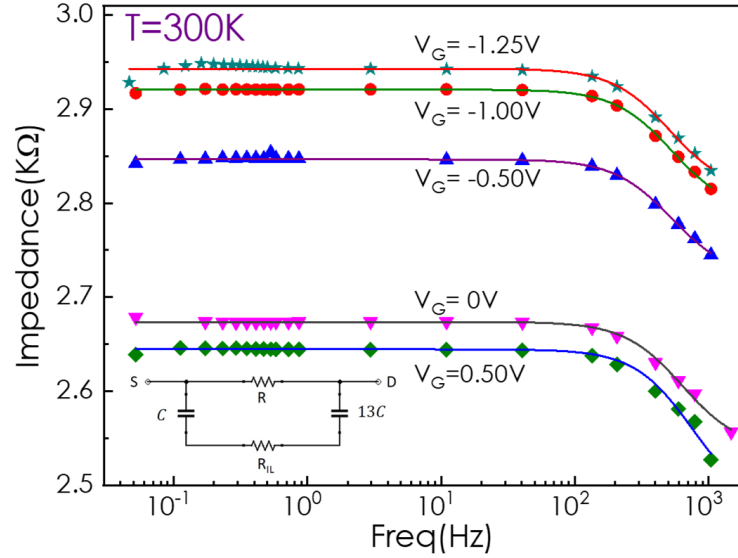


FIG. 5. (a) Frequency dependence impedance of InN thin film at different mentioned gate voltages. Solid lines are the fits using circuit models shown in the inset of Figure. R , R_{IL} are the resistances of the sample and ionic liquid respectively.

TABLE I. Capacitance and resistances of ionic liquid for different applied gate voltages obtained from EIS.

V_G	Capacitance($\mu F/cm^2$)	R_{IL} (k Ω)
0.5	4.84	38.6
0	4.5	50
-0.5	4.4	61.8
-1	4.33	61.9
-1.25	4.45	62.6

-
- [1] K. Ghosh, J. S. Rathore, and A. Laha, [Superlattices and Microstructures](#) **101**, 405 (2017).
 - [2] H. Yuan, H. Shimotani, A. Tsukazaki, A. Ohtomo, M. Kawasaki, and Y. Iwasa, [Advanced Functional Materials](#) **19**, 1046 (2009).
 - [3] T. Sato, G. Masuda, and K. Takagi, [Electrochimica Acta](#) **49**, 3603 (2004).
 - [4] T. A. Petach, M. Lee, R. C. Davis, A. Mehta, and D. Goldhaber-Gordon, [Physical Review B](#) **90**, 081108 (2014).
 - [5] R. Misra, M. McCarthy, and A. F. Hebard, [Applied Physics Letters](#) **90**, 052905 (2007).